Available online at www.sciencedirect.com
SCIENCE DIRECT®
International Journal of Refrigeration 27 (2004) 464–474
REVUE INTERNATIONALE DU FROID
INTERNATIONAL JOURNAL OF
refrigeration
www.elsevier.com/locate/ijrefrig

Airflow pattern and temperature distribution in a typical refrigerated truck configuration loaded with pallets

J. Moureh[a,*], D. Flick[b]

[a]UMR Génie Industriel Alimentaire Cemagref-ENSIA-INAPG-INRA, Refrigerating Process Engineering Unit, Parc de Tourvoie, Cemagref, BP 44, 92163 Antony cedex, France
[b]UMR Génie Industriel Alimentaire Cemagref-ENSIA-INAPG-INRA, INA-PG, 16, rue Claude Bernard, 75005 Paris, France

Received 14 November 2003; received in revised form 29 January 2004; accepted 26 February 2004

Abstract

This work is part of a research activity aiming to improve and to optimise air-distribution systems in refrigerated vehicles in order to decrease the temperature differences throughout palletised cargos. This condition is essential in order to preserve the quality, safety and shelf life of perishable products. The present study reports on the numerical and experimental characterization of airflow within a semi-trailer enclosure loaded with pallets. The experiments were carried out on a reduced-scale (1:3.3) model of a refrigerated-vehicle trailer. The performance of ventilation and temperature homogeneity were characterized with and without supply air duct systems. Both configurations are extensively used in refrigerated transport. The numerical modelling of airflow was performed using the Computational Fluid Dynamics (CFD) code Fluent and a second-moment closure, the Reynolds stress model (RSM). The results obtained using the RSM model showed good agreement with the experimental data. Numerical and experimental results clearly show the importance of air ducts in decreasing temperature differences throughout the cargo.

Keywords: Refrigerated transport; Air distribution; Temperature variation; Modelling; Pallet

Ecoulement d'air et niveaux de température dans un véhicule frigorifique chargé de palettes

Mots-clés: Transport frigorifique; Distribution d'air; Variation de température; Modélisation; Palette

1. Introduction

During transport using refrigerated vehicles, this being an important link in the cold chain, the maintenance of even temperature throughout the cargo is essential in order to preserve the quality, safety and shelf life of perishable food Within the refrigerated enclosure, the temperature level and its homogeneity are directly governed by airflow patterns. The design of the air-distribution system should allow these airflows to compensate heat fluxes exchanged through the insulated walls or generated by the products. This process is essential in order to decrease temperature differences throughout the cargo.

In the refrigerated vehicle enclosure (RVE), the air is supplied at relatively high velocities through a small inlet section located adjacent to or near the ceiling. Due to the Coanda effect, this design should allow the confined wall jet produced to directly remove, as far as possible, the heat

* Corresponding author. Tel.: +33-140-96-60-88; fax: +33-140-96-62-49.
E-mail address: jean.moureh@cemagref.fr (J. Moureh).

0140-7007/$35.00 © 2004 Published by Elsevier Ltd and IIR.
doi:10.1016/j.ijrefrig.2004.03.003

Nomenclature

C_p,	specific heat of air (J kg^{-1} K^{-1});
C_μ,	turbulence model coefficients;
D_H,	hydraulic diameter of the inlet section (m);
e,	air spaces separation between wall and pallets (m);
H,	height of the truck (m);
I,	turbulence intensity (%);
L,	length of the truck (m);
p,	static pressure (Pa);
P,	production term (m^2 s^{-3});
Q,	flow rate (m^3 s^{-1});
Re,	Reynolds number, Re $= \rho U_0 D_H/\mu$;
T, t,	mean, fluctuating temperature (K);
T_e,	external temperature (K);
$\overline{u_i u_j}$,	Reynolds stress component (m^2 s^{-2});
z_0,	separation point coordinate (m);
U_i, u_i,	mean and fluctuating velocity component in x_i direction (m s^{-1});
V,	velocity magnitude (m s^{-1});
x, y, z,	lateral, vertical and longitudinal coordinates (m)

Greek symbols

ρ,	density (kg m^{-3});
ν,	kinematic viscosity (m^2 s^{-1});
μ,	dynamic viscosity (kg m s^{-1});
k,	kinetic energy of turbulence (m^2 s^{-2});
ε,	turbulence energy dissipation rate (m^2 s^{-3});

Subscript

0	inlet
mad	maximum
min	minimum
t	turbulent
i, j, k	vector directions in x, y and z

fluxes exchanged by the walls. From an aerodynamic standpoint, the principal particularity of this configuration is the presence of blowing and suction sections of airflow on the same face since it is very practical to bring together all the refrigerated equipment on the front side near the refrigerating unit. The drawback of this asymmetrical airflow design is the presence of a strong pathway between the two sections, implying high velocities in the front of the RVE. In addition, the compactness of the cargo and high resistance to airflow due to thin air spaces between pallets result in uneven air distribution in the cargo where stagnant zones with poor ventilation can be observed in the rear part of the vehicle. In these zones, higher temperatures can occur locally within the load [1–5] even though the refrigerating capacity is higher than heat fluxes exchanged by the walls and the products [6].

Recent investigations showed that little or no research on the characterization of air velocities in a truck loaded with pallets has been performed. This can be attributed to the complexity of direct measurement of local air velocities and flow rates in the thin air spaces located between pallets and boxes. However, an experimental approach used by Lindqvist [7,8] to measure pressure inside a full-scale laboratory model of a reefer hold loaded with pallets showed very poor distribution of airflow within the vessel. The same study also showed that high pressure gradients reflecting high velocities were located in the front of the vessel, and in contrast, weak pressure gradients/or velocities were present at the rear of the vessel.

Several modelling approaches using electrical analogies to predict the airflow rate in spacing or channels between pallets or boxes were developed by Wang and Touber [9], Meffert and Van Beek [10] and Zertal-Ménia et al. [11]. These approaches could give qualitative information on the air circulation rate and do not require much time or memory capacity. However, these simplified modelling approaches were not able to provide quantitative predictions of airflow patterns, local air velocities and turbulence levels, which are important in heat transfer phenomena. In addition, predictions cannot take into account the behaviour, the stability and the diffusion of the supplied forced air jet.

Numerical predictions of air velocities and temperature distributions can be obtained by solving sets of differential equations of mass, momentum and energy written in their conservative form using the finite-volume method. Using Computer Fluid Dynamics (CFD) codes, computers and processing facilities, complex configurations such as refrigerated transport or storage have been studied by many authors [12,13].

Van Gerwen and Van Oort [13] used the Phoenics CFD package to predict air velocities and product temperature based on cooler airflow rate, product properties and the geometry of cold store and stowage pattern. In this model, the authors gave design recommendations in order to better homogenize airflow circulation and temperature levels in the load. However, no data were given by the authors concerning the numerical approach, the turbulence model, the boundary conditions, the experimental and numerical data, the validation procedure and its accuracy. Consequently, such models are difficult to evaluate.

More recently, Hoang et al. [14] used the CFX CFD package code to predict the airflow pattern in empty and loaded cold stores. The forced-circulation air cooler unit was modelled using an appropriate body force and resistance, corresponding to the characteristics of the fan and the tube bank-evaporator. Validation was performed by comparisons of numerical and experimental data on vertical profiles of air velocity magnitudes. The accuracy was 26% for the standard $k-\varepsilon$ model and 28.5% for the RNG model. According to the authors, the Coanda effect governing the attachment of the jet on the ceiling was not well predicted by the $k-\varepsilon$ model. Moreover, validation of this model lacks

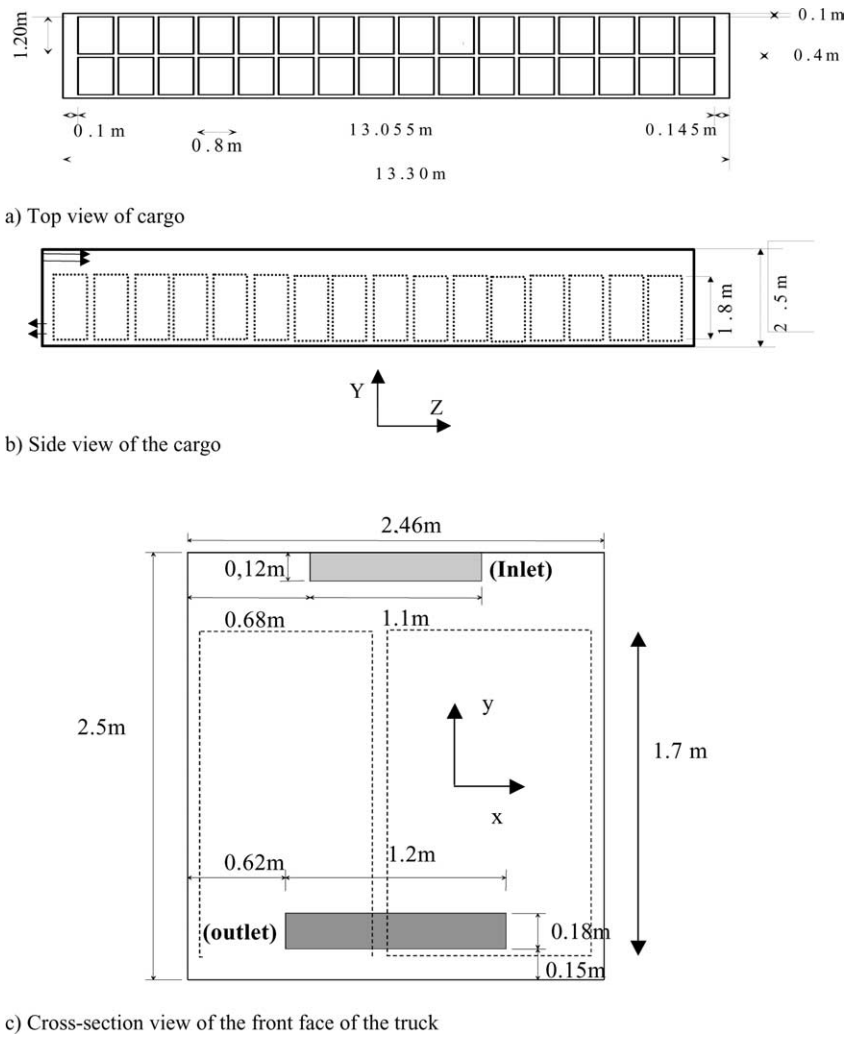

Fig. 1. Dimensions of the vehicle configuration investigated.

comparisons between numerical and experimental data regarding such aspects as airflow patterns, diffusion of the jet leaving the cooler and turbulence profiles.

Many studies use the $k-\varepsilon$ model since it is easy to programme and has good stability and broad applicability. However, predictions given by this model are often not accurate and modifications are performed in order to improve the computed results, especially in empty slot-ventilated enclosures where experimental data are easier to obtain. To improve numerical predictions, Choi et al. [15] suggested modifying the multiplicator coefficient $C_\mu = 0.09$ of the turbulent viscosity given by the standard $k-\varepsilon$ model. In a comparison of different $k-\varepsilon$ models for indoor airflow, Chen [16] showed that all these models studied were unable to predict the presence of the secondary recirculating flow. These poor predictions given by the $k-\varepsilon$ model can be attributed to the complexity of the airflow in a room since it is often the combination of free turbulent shear flows, near wall effects, pressure gradients implying the presence of local separation and secondary flows including high streamline curvature effect [15–21]. In addition, a more complicated and complex system can be expected due to the presence of the load. For such complex flows, fundamental studies [22–24] agree on the inadequacy of the $k-\varepsilon$ model and underline its limitations by comparison with experimental data. In this case, improving predictions can be achieved by taking into account the effect of the turbulence anisotropy by using models based on the second-moment closure.

The objective of this study was to investigate numerically and experimentally the airflow pattern throughout a vehicle enclosure loaded with two rows of pallets with and without an air duct system. The model developed was investigated using the CFD code Fluent and second-moment closure with the Reynolds stress model as described by Launder et al. [25]. To validate the model, predicted values

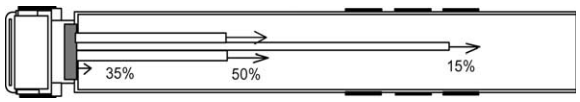

Fig. 2. Schematization of air ducts and airflow distribution in the truck.

of velocity and airflow patterns were compared with experimental data obtained on a scale model under isothermal conditions. After adequate validation, the model could be used as a design tool to optimise more complex configurations, reducing the need for expensive and time-consuming experiments.

2. Experimental device

The experiments were carried out using a reduced-scale (1:3.3) model of a refrigerated-vehicle trailer with respect to the adimensional Reynolds number. Afterwards, all the data—dimensions, flow rate and results—are expressed for the actual scale. The walls of the scale model are made of wood. Only one lateral wall is made of glass to allow internal air velocity measurement using laser Doppler velocimetry. The blowing and outlet sections are located on the same side at the front of the trailer. Inside the scale model, closed glass boxes are used to represent pallets. The loaded configuration consists of two rows of 16 pallets. The dimensions of this device expressed using the actual scale are represented in Fig. 1.

The mean velocity and its fluctuations were obtained with a one-dimensional laser-Doppler anemometer placed outside the model in order to avoid interference with the flow. It comprised a 50 mW laser diode emitting a visible red beam at 690 nm wavelength, a Beamsplitter, a Brag cell, a focussing and receiving lens and a pinhole arrangement to collect scattered light from within the measurement value and a photomultiplier. Light scattered from particles is captured through the same front lens that the two beams exit from. The air supplied to the model trailer was passed through atomizers and allowed near continuous Doppler signals which were converted into velocity and time.

In addition to the empty truck, two loaded configurations were investigated:

(i) Without air ducts. The whole airflow rate is blown at the front of the truck (Fig. 1). In this configuration, two air spaces distances between pallets and walls are considered: the reference case with $e = 2$ cm and $e = 1$ cm.
(ii) With air ducts. The airflow rate was blown on three positions: $x = 0$ (front), $x = L/3$, $x = 3L/4$ with 35, 50 and 15% as the flow rate proportions, respectively (Fig. 2).

Unless stated otherwise, the results presented are related to the reference case.

3. Numerical modelling

3.1. Governing equations and hypothesis

The description of temperature and airflow development are based on the conservative law of mass, motion and energy. Natural convection is considered by using the Boussinesq approximation in which density was treated as a constant value in all solved equations except for the buoyancy term in the momentum equations which was treated as: $(\rho_0 - \rho)g = \rho_0\beta(T - T_0)g$, where ρ_0 and T_0 are the reference density and temperature respectively, and β is the thermal expansion coefficient. The solved equations can be written as follows:

Mass conservation:

$$\frac{\partial U_j}{\partial x_j} = 0 \tag{1}$$

Momentum conservation:

$$\frac{\partial U_j U_i}{\partial x_j} = -\frac{1}{\rho}\frac{\partial P}{\partial x_i} + \frac{\partial}{\partial x_j}\left(\nu\frac{\partial U_i}{\partial x_j} - \overline{u_i u_j}\right) \tag{2}$$

Energy conservation:

$$\frac{\partial U_j T}{\partial x_j} = \frac{\partial}{\partial x_j}\left(\frac{\nu}{\mathrm{Pr}}\frac{\partial T}{\partial x_j} - \overline{u_j t}\right) \tag{3}$$

where $\overline{u_i u_j}$ and $\overline{u_j t}$ are, respectively, the unknown Reynolds stresses and heat fluxes. The obtaining of these quantities depends on the turbulence closure. For the case investigated, the second-moment closure with the Reynolds stress model (RSM) is used.

The transport equations for Reynolds turbulent stress can be written as:

$$U_k\frac{\partial \overline{u_i u_j}}{\partial x_k} = -\frac{\partial}{\partial x_k} \times\left[\overline{u_i u_j u_k} + \frac{p}{\rho}(\delta_{kj}u_i + \delta_{ik}u_j) - \nu\frac{\partial(\overline{u_i u_j})}{\partial x_k}\right] + P_{ij} - \overline{\frac{p}{\rho}\left[\frac{\partial u_i}{\partial xj} + \frac{\partial u_j}{\partial xi}\right]} - 2\nu\overline{\frac{\partial u_i}{\partial x_k}\frac{\partial u_j}{\partial x_k}} \tag{4}$$

where

$$P_{ij} = -\overline{u_i u_k}\frac{\partial U_j}{\partial x_k} - \overline{u_j u_k}\frac{\partial U_i}{\partial x_k}$$

represents the production term.

The diffusive transport term was represented by a simplified form of the generalized gradient diffusion hypothesis as:

$$-\frac{\partial}{\partial x_k}\left[\overline{u_i u_j u_k} + \frac{p}{\rho}(\delta_{kj}u_i + \delta_{ik}u_j) - \nu\frac{\partial(\overline{u_i u_j})}{\partial x_k}\right] = \frac{\partial}{\partial x_k}\left(\frac{\nu_t}{\sigma_k}\frac{\partial}{\partial x_k}(\overline{u_i u_j})\right) \tag{5}$$

The pressure-strain term consisted of the linear return-to-isotropy and is modelled by Launder et al. [25] as:

$$\overline{\frac{p}{\rho}\left[\frac{\partial u_i}{\partial xj}+\frac{\partial u_j}{\partial xi}\right]} = -C_1\frac{\varepsilon}{k}\left[\overline{u_iu_j}-\frac{2}{3}\delta_{ij}k\right]-C_2\left[P_{ij}-\frac{2}{3}\delta_{ij}P\right] \quad (6)$$

where the constants $C_1 = 1.8$ and $C_2 = 0.60$, and $P = 0.5P_{ii}$.

The dissipation term, assumed isotropic, was approximated by:

$$2\nu\overline{\frac{\partial u_i}{\partial x_k}\frac{\partial u_j}{\partial x_k}} = \frac{2}{3}\delta_{ij}\varepsilon$$

where the dissipation rate was computed via the ε transport equation.

$$U_i\frac{\partial \varepsilon}{\partial x_i} = \frac{\partial}{\partial x_i}\left[\left(\nu+\frac{\nu_t}{\sigma_\varepsilon}\right)\frac{\partial \varepsilon}{\partial x_i}\right]+\frac{\varepsilon}{k}(C_1f_1P_k - C_2f_2\varepsilon) \quad (7)$$

The turbulent heat flux was expressed as:

$$\overline{u_jt} = -\frac{\partial}{\partial x_j}\left(\frac{\nu_t}{\mathrm{Pr}_t}T\right) \quad (8)$$

3.2. Boundary conditions

Since the geometrical model is symmetric, only half the domain of flow field is actually simulated. The computational domain may be surrounded by inflow and outflow boundaries in addition to symmetry and solid walls.

At the inlet, uniform distribution is assumed for velocity components, kinetic energy of turbulence k_0 and the energy dissipation rate, ε_0. The numerical values are specified as:

- ($U_{0x} = U_{0y} = 0$; $U_{0z} = U_0 = 11.5$ m/s representing the mean longitudinal velocity, giving an inlet flow rate $Q_0 = 5500$ m^3/h;
- $k_0 = 3/2(U_0I_{0z})^2$; where I_{0z} represents the turbulence intensity of the z-component of velocity at the inlet;
- $\varepsilon_0 = (C_\mu^{0.75}k_0^{1.5}/0.07D_H)$ where D_H represents the hydraulic diameter of the inlet section;
- $\overline{u_iu_j} = \frac{2}{3}k_0\delta_{ij}$ for the RSM model, where turbulence is assumed to be isotropic.

According to these conditions, the Reynolds number is considered as being equal to 2×10^5 in experiments and numerical simulations. At the outflow, pressure is supposed to be uniform and zero-gradient is applied for all transport variables.

The turbulence models are only valid in fully turbulent regions. Close to the wall, where viscous effects become dominant, the model is used in conjunction with wall functions. For this study, the conventional equilibrium logarithmic law governing the wall is used [26].

At the symmetry plane, zero normal velocity and zero normal gradients of all variables are assigned.

The computations are performed in a stationary regime using FLUENT, a commercial computational-fluid dynamics (CFD) code on a three-dimensional configuration. The governing equations are solved using the finite-volume method in a staggered grid system. Non-uniform grid distribution is used in this study, with finer grid in regions near the inlet, outlet and walls where high gradients are expected. In these simulations, the quick scheme, based upon three-point upstream-weighted quadratic upstream interpolation rather than linear interpolation between consecutive grid points [27] is used. The principal objective in using the quick scheme is to reduce the grid size required to yield a grid-independent solution, in comparison to the low-order scheme.

In this study, the grid selected for the results presented below was very fine, with $50\times52\times240$ grid cells representing half depth (1.23 m) × height (2.5 m) × length (13.3 m), which was equal to 624,000 cells for the empty configuration and 419,000 cells for the loaded configuration as the load is not part of the modeled domain. The computation time was approximately 3 days. It was conducted on a personal computer equipped with a 450 MHz processor.

However, a lot of simulations made with coarser grids, not presented here, show for greater than 350,000 cells that the predicted values are grid-independent.

All figures presented below are related to the reference case unless otherwise stated.

For thermal simulations, the following boundary coefficient conditions were assumed:

- External temperature $T_e = 30$ °C
- Blowing temperature $T_0 = -28$ °C
- Overall heat transfer through the insulating wall: 0.3 W/m^2 K
- The pallets are considered to be adiabatic. Only convective exchange between the truck wall and the air is taken into consideration.

4. Results and discussion

4.1. Airflow comparisons between empty and loaded configurations

Fig. 3 shows a comparison between empty and loaded configurations concerning the streamlines related to the mean flow field in the symmetry plane. In empty configuration, Numerical and experimental data show that the jet separates at approximately 10 m from the inlet which corresponds to $z_0 = 0.75L$. In a shorter configuration ($L/H < 2.5$), Adre and Albright [28] and Yu and Hoff [29] obtained $z_0 = 0.64L$ and $0.84L$ respectively as the location of the separation point. In addition, all these studies are in

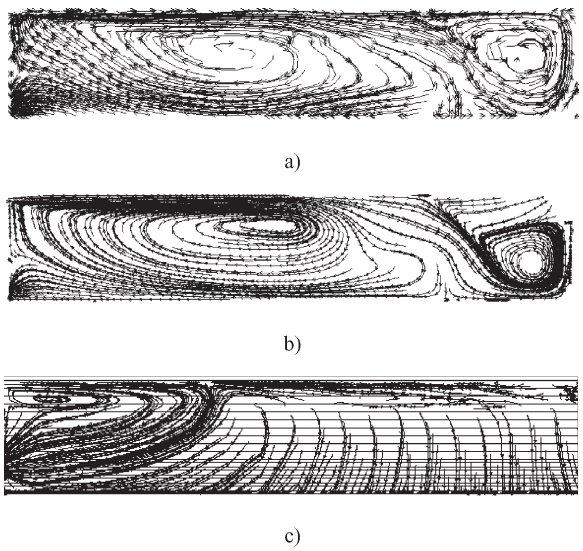

Fig. 3. Streamlines in symmetry plane. (a) Empty configuration: experimental values using LDV with 1100 measurement points. (b) Empty configuration: RSM model. (c) Loaded configuration: RSM model.

agreement with the fact that the separation point remains constant above a threshold Reynolds number value.

This separation splits the jet into two regions dominated by two vortices of opposite circulation. The primary recirculation located on the front part of the enclosure delimits the reach and the action of the inlet jet. Conversely, the secondary flow located at the rear part is weakly supplied by the primary jet. In addition, the velocities are very low. According to Moureh and Flick [21], the separation of the jet from the wall is due to the confinement effect and to the presence of an adverse pressure gradient along the enclosure.

To illustrate the effect of confinement on the ventilation efficiency of the wall jet into the truck, Fig. 4 shows a comparison between empty and loaded configurations concerning the longitudinal evolution along the truck of the dimensionless airflow rate ($Q(z)/Q_0$), obtained using numerical data. For a given cross-section along the enclosure, the circulating flow rate $Q(z)$ was calculated as follows:

$$Q(z) = 0.5 \int_{S_{(z)}} |U_z| \mathrm{d}s \tag{9}$$

where $S_{(z)}$ represents the cross-section considered at z coordinate and U_z represents the local longitudinal velocity normal to $S_{(z)}$.

In a comparison with an unbounded wall jet, the confinement effect naturally reduces the development of the jet and the entrainment phenomena with the surrounding ambience [30]. In an empty configuration, the confinement is due to the wall boundaries of the enclosure. In a loaded configuration, the presence of pallets significantly increases the confinement effect. Consequently, the evolution of adimensional airflow rate ($Q(z)/Q_0$) in the loaded configuration is lower than in the empty configuration. According to Fig. 4, the maximum values of ($Q(z)/Q_0$) are 1.5 for loaded configuration and 3 for empty configuration and they are reached at 1 m and 3.5 m respectively. As a result, the jet decays more rapidly in loaded configuration than empty one (Fig. 5). Thus, the separation point is located further upstream ($z_0 = 0.45L$) and the primary recirculation zone is more reduced (Fig. 3(c)).

The comparisons between numerical and experimental results (Figs. 3 and 5) show the ability of the RSM model to correctly predict the decay of the wall jet, the location of the separation point, the aerodynamic characteristics of primary and secondary recirculations and the overall behaviour of airflow patterns. These figures also illustrate the heterogeneity of ventilation between the front and the rear parts of the truck.

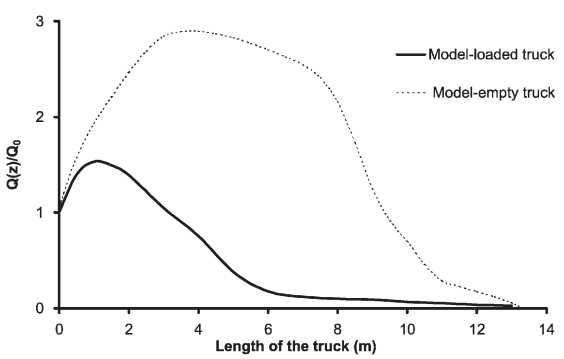

Fig. 4. Longitudinal evolution along the truck of the dimensionless airflow rate ($Q(z)/Q_0$) in empty and loaded configurations.

4.2. Airflow behaviour and velocity characteristics above the pallets

In order to illustrate the overall behaviour of the airflow above the pallets, experimental and numerical contours of

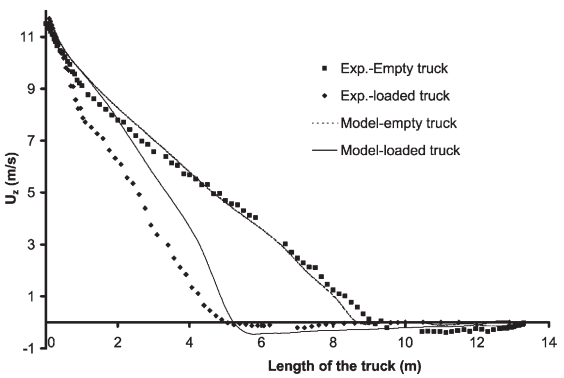

Fig. 5. Comparisons between numerical and experimental results concerning the decay of the jet longitudinal velocity along the blowing medium line in empty and loaded configurations.

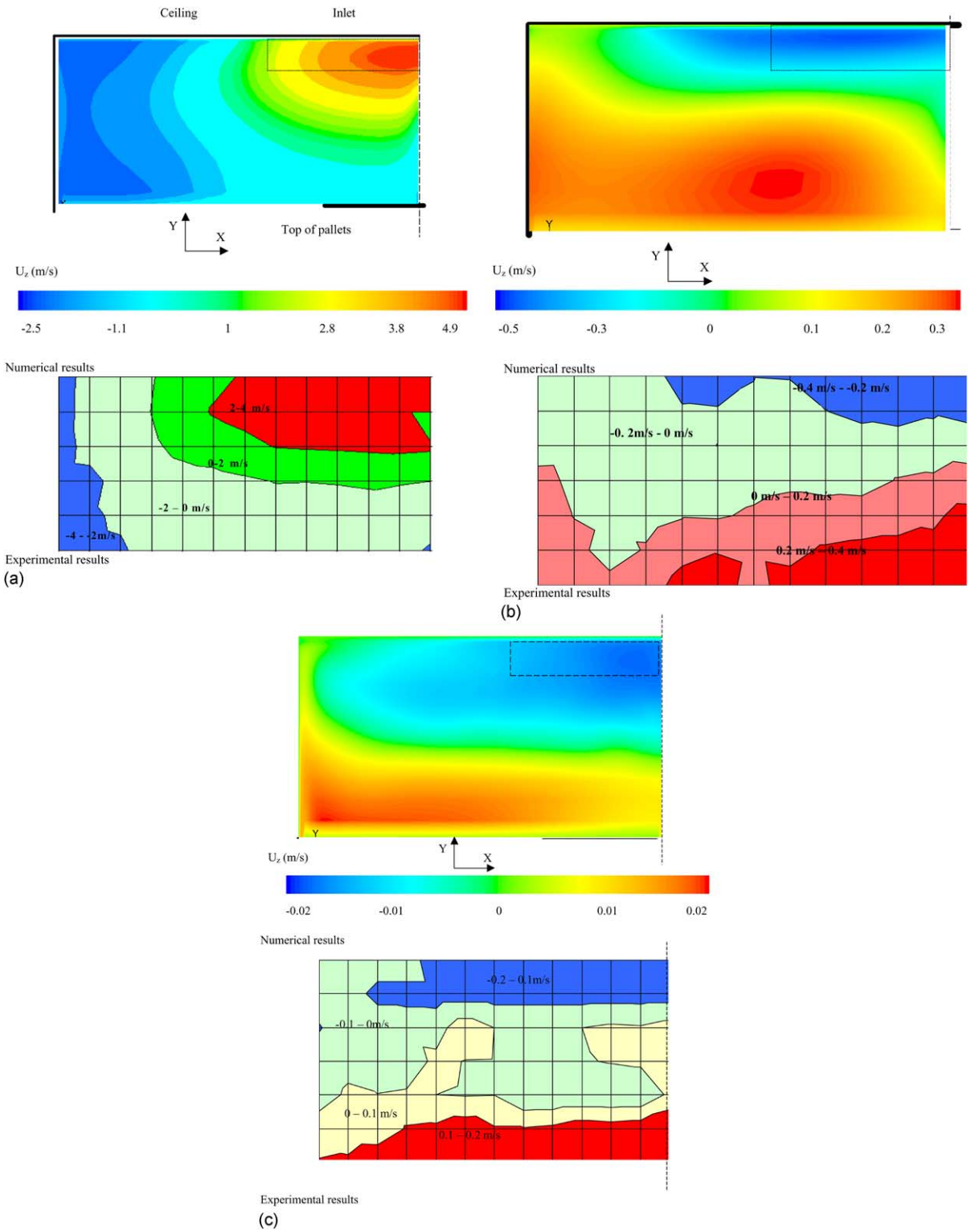

Fig. 6. Velocity field above the loading at $L/4$ (a), $L/2$ (b) and $3L/4$ (c): comparisons between numerical and experimental data.

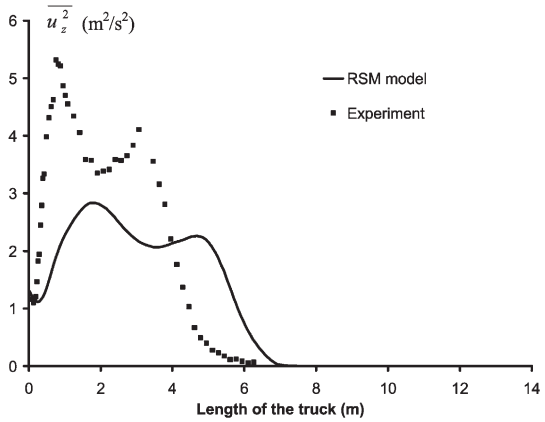

Fig. 7. Evolution of the mean-square of the turbulent velocity in the z direction ($\overline{u_z^2}$) along the truck.

velocity fields are presented and compared on Fig. 6 in three cross-sections at $L/4$, $L/2$ et $3L/4$ of the vehicle. Each figure was obtained from 90 experimental points.

At $L/4$ (Fig. 6(a)) velocity fields show that the wall jet moved along the ceiling where is maintained by the Coanda effect and returns along the side walls and above the pallets. Near side walls velocities are very low and negative.

In the middle of the vehicle (Fig. 6(b)), located downstream of the separation of the wall jet, the behaviour of the airflow is completely different. After its separation from the wall, the jet reattaches on the top of the pallets where velocities become positive. Simultaneously, the jet returns along the ceiling where the velocities are negative.

At $3L/4$, (Fig. 6(c)), velocities still positive above the pallets and negative on the ceiling where the returning airflow occupies the whole width.

Despite the complexity of the airflow illustrated by these three mappings, with the separation of the jet from the wall and its reattachment on the top of the pallets, the RSM model shows good agreement with experimental data.

4.3. Turbulence behaviour

Fig. 7 shows comparisons between numerical and experimental data concerning the evolution of the mean-square of the turbulent velocity in the z direction ($\overline{u_z^2}$) through the inlet section along the enclosure in a loaded configuration. Overall, we observe high values of $\overline{u_z^2}$ in the front half of the vehicle where numerical and experimental curves show two peaks. The first peak is a common characteristic of turbulent jet expansion due to diffusion of the turbulence from the edge to the core of the jet. The second peak located near the separation area of the jet from the wall reflects the extra amount of turbulence generated in this region where high velocity gradients were locally present. Even if the trends of numerical and experimental values are similar, the RSM model seemed to overestimate the diffusive character of the turbulence. Consequently, predicted peak values of $\overline{u_z^2}$ were obviously lower than experimental data. This figure also shows very low values of kinetic energy, close to zero, in the rear half of the vehicle. This indicates low velocities and the low air movement in this area.

Fig. 8 shows a comparison between numerical and experimental data concerning the $\overline{u_z^2}$ field values in a cross-section at $L/4$ above the pallets. High turbulence near the jet boundaries of the mixing area and low values for the returning flow under the jet and near the wall boundaries can be seen.

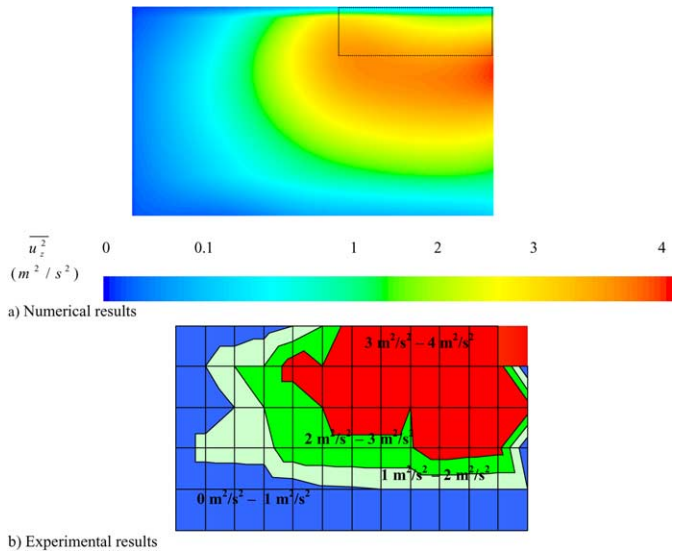

Fig. 8. Contours of the mean-square of the turbulent velocity in the z direction ($\overline{u_z^2}$) above the loading at $L/4$: comparisons between numerical and experimental data.

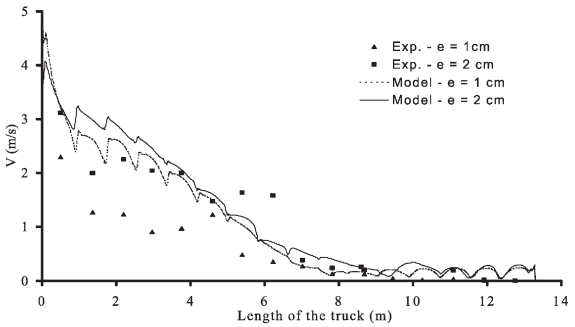

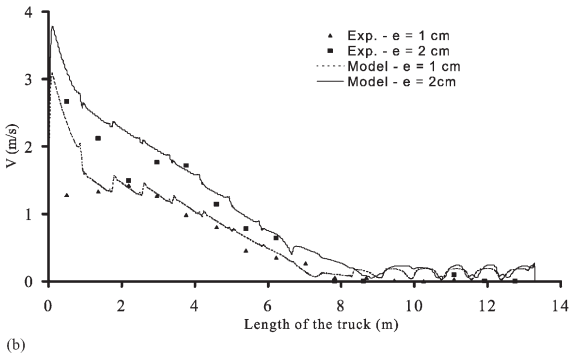

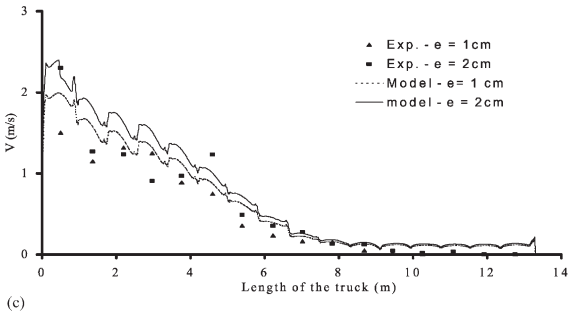

Fig. 9. Evolution of air velocity magnitude between the lateral wall and pallets at three levels top (a), middle (b) and bottom (c) of pallets along the truck for $e = 1$ and 2 cm.

4.4. Influence of air space thickness between wall and pallets

The thin air space ($e = 1-2$ cm) located between lateral wall and pallets (Fig. 1) represents the most sensitive area in the load. As regards the low velocities between the wall and the pallets, heat fluxes exchanged through the insulated wall with the surrounding atmosphere are difficult to remove in this space and high temperatures are expected locally.

Fig. 9 presents a comparison between numerical and experimental data concerning velocity magnitude at three levels on pallets: high, medium and at the bottom along the enclosure for two air spaces: 1 and 2 cm. These figures clearly show that in these spaces the air velocity magnitudes

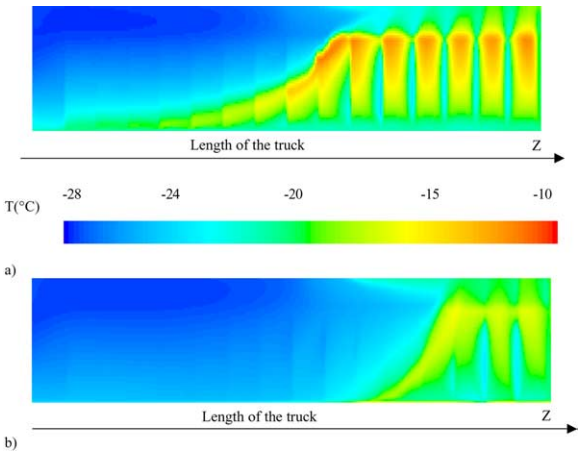

Fig. 10. Numerical results concerning contours of iso-temperatures in the most sensitive plane of the truck located between lateral wall and pallets for $e = 1$ and 2 cm.

were governed by the behaviour of the air wall jets and the presence of primary and secondary recirculations. Downstream from the separation of the jet, beyond 6 m from the inlet, the velocities are very low and close to zero. Conversely, high velocities correspond to the zone of primary recirculation. It is interesting to note that for $e = 2$ cm, velocities are overall higher than 1 cm. This underlines the importance of this separation to improve the ventilation efficiency in this area and thus reduce temperature levels. We also noted the good qualitative agreement between numerical and experimental data.

Fig. 10 presents a numerical comparison concerning the contours of air temperatures in this plane for these two air spaces: 1 and 2 cm. As expected, higher velocities obtained with $e = 2$ cm allow to significantly reduce temperature levels in this area. However, these numerical results should be interpreted with caution because it cannot be verified experimentally on the isothermal reduced scale model. This result agrees with Nordtverdt [31] who recommends maintaining air spaces between pallets and walls in order to improve ventilation and to reduce temperature differences.

4.5. Influence of the air duct on airflow and temperature distribution

Fig. 11 shows a comparison with and without the use of air ducts concerning (from numerical data given by the RSM model) the longitudinal evolution along the truck of the dimensionless airflow rate ($Q(z)/Q_0$), obtained by numerical data. This result clearly shows that ventilation of the rear of the truck is improved by the use of air ducts. In this area, the flow rate is increased from 100 to 1000 m^3/h approximately. Conversely, it is reduced at the front of the truck. This reflects a better uniformity of the ventilation in the truck.

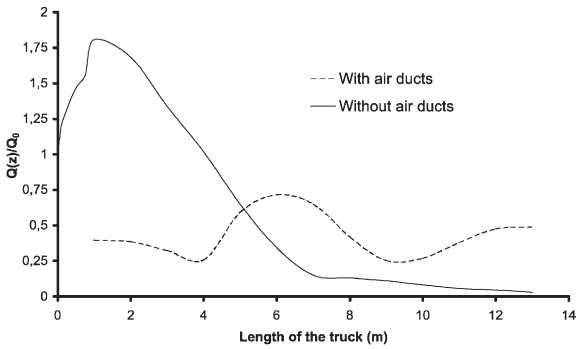

Fig. 11. Longitudinal evolution along the truck of the dimensionless airflow rate ($Q(z)/Q_0$) with and without air ducts.

Fig. 12 presents a comparison between experimental and predicted values of air velocities at medium level between wall and pallets with and without an air duct. These figures clearly show that in these spaces the air velocity magnitudes were governed by the behaviour of the overall airflow rate. As observed in numerical and experimental results, the use of air ducts improves air circulation and its homogeneity along this sensitive plane. The most important is to avoid the occurrence of low velocities and a stagnant zone in the rear part of the truck where velocities are maintained at around 1 m/s instead 0.1 m/s without this device.

To evaluate the benefit of air duct on temperature levels and their uniformity, Fig. 13 presents a numerical comparison concerning the contours of air temperatures in this most sensitive plane with and without this device. As it can be seen, when air ducts are used, the zones of higher temperature moves from the rear of the truck to the middle position located between two air duct nozzles where lower velocity is expected. The use of an air duct makes it possible to decrease the higher temperature (T_{max}) from − 16 °C to − 20 °C. In addition, the dispersion of of the air temperature, defined as ($T_{max} - T_{min}$), decreases from 12 K for a vehicle without air ducts to 8 K for a vehicle with air ducts.

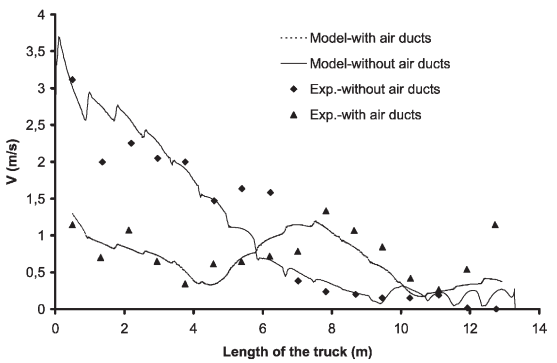

Fig. 12. Evolution of air velocity magnitude between lateral wall and pallets at the middle level with and without air ducts.

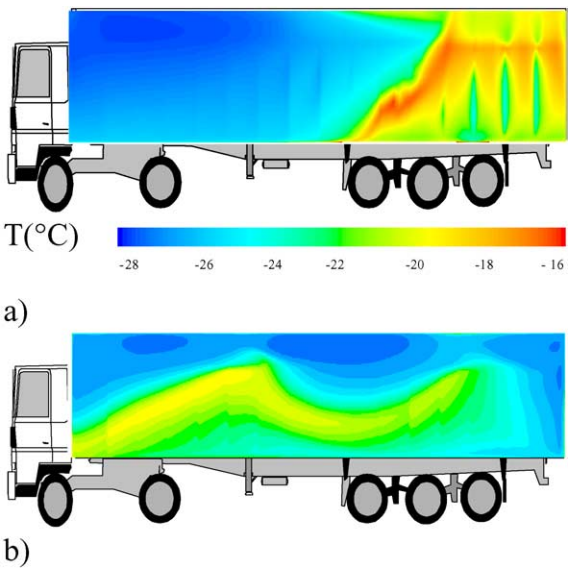

Fig. 13. Numerical results concerning contours of iso-temperatures in the most sensitive plane of the truck located between lateral wall and pallets with and without air ducts.

5. Conclusion

In this study, experiments and numerical simulations performed using the computational fluid dynamics code Fluent were carried out in order to characterize velocities, airflow patterns and temperature levels within a typical loaded vehicle with and without a duct air supply system. The experiments were carried out on an isothermal reduced-scale model with laser-Doppler velocimetry.

Experiments and simulations highlight the importance of the load and confinement effect in reducing the reach of the jet for which the separation occurs at 6 m from the inlet. This separation maintains a high degree of ventilation heterogeneity between the front and the rear where stagnant zones and low velocities are present.

The simulations show the ability of the RSM model to accurately predict the local separation of the jet from the wall and and the overall behaviour of airflow patterns and velocity characteristics. There was good prediction also in the thin air space separation (1–2 cm) between pallets and walls, which constitutes the most sensitive plane in the load. The results also underline the importance of these separations in maintaining the ventilation around the pallets in order to better remove heat exchanged through insulated walls and thus to decrease the higher temperatures reached locally in this most sensitive area.

Numerical and experimental results show that the use of air-duct systems improves the overall homogeneity of the ventilation in the truck and avoids the occurrence of stagnant zones and low velocities in the rear part of the load. In this zone, velocities are maintained at around 1 m/s instead of 0.1 m/s without this air duct. These aspects

contribute to a decrease in the temperature differences throughout the palletised cargo and thus to the preservation of the quality, safety and shelf life of perishable products.

References

[1] Lenker DH, Wooddruff DW, Kindya WG, Carson EA, Kasmire RF, Hinsch RT. Design criteria for the air distribution systems of refrigerated vans. ASAE Pap 1985;28(6):2089–97.

[2] Gögus AY, Yavuzkurt S. Temperature pull-down and distribution in refrigerated trailers. I.I.F—I.I.R commissions D2; 1974. p. 189–93.

[3] LeBlanc D, Beaulieu C, Lawrence R, Stark R. Evaluation of temperature variation of frozen foods during transportation. Refrigeration Res Found Inf Bull 1994;december. Bethesda, Maryland, USA.

[4] Bennahmias R, Labonne G. Etude de la distribution de l'air et de la dispersion des températures dans une semi-remorque frigorifique. Réunion des commissions C2, D1 et D2/3 de l'IIF, Fez (Morocco) 1993;241–56.

[5] Meffert HFTh, Van Nieuwenhuizen G. Temperature distribution in refrigerated vehicles. Proceedings I.I.F.—I.I.R, Commissions D1, D2 and D3, Barcelona, Spain. 1973. p. 131–5.

[6] Billiard F, Bennahmias R, Nol P. Nouveaux développements dans les transports à température dirigée routiers. Proceedings I.I.F.–I.I.R. Commissions B2, C2, D1, D2/3, Dresden, Germany. 1990. p. 793–802.

[7] Lindqvist R. Reffer Hold Distribution. Preprint Conferences. I.I.F./I.I.R., Cambridge UK. 1998.

[8] Lindqvist R. Air distribution design for controlled atmosphere in reefer cargo holds. 20th International Congress of Refrigeration, IIR/IIF, Sydney. 1999.

[9] Wang H, Touber S. Simple non-steady state modelling of a refrigerated room accounting for air flow and temperature distributions. Proceedings I.I.F.–I.I.R. Commissions B1, B2, C2, D1, D2/3, Wageningen. 1988. p. 211–9.

[10] Meffert HFTh, Van Beek G. Basic elements of a physical refrigerated vehicles, air circulation and distribution. 16th International Congress of Refrigeration, I.I.F.–I.I.R., Paris. 1983. p. 466–75.

[11] Zertal-Ménia N, Moureh J, Flick D. Modélisation simplifiée des écoulements d'air dans un véhicule frigorifique. Int J Refrigeration 2002;25:660–72.

[12] Wang H, Touber S. Distributed dynamic modelling of a refrigerated room. Int J Refrigeration 1990;13:214–22.

[13] Van Gerwen RJM, Van Oort H. Optimization of cold store using fluid dynamics models. Proceedings I.I.F.–I.I.R. Commissions B2, C2, D1, D2/3, Dresden, Germany, vol. 4.; 1990. p. 473–80.

[14] Hoang ML, Verboven P, De Baermaeker J, Nicolaï BM. Analysis of air flow in a cold store by means of computational fluid dynamics. Int J Refrigeration 2000;127–40.

[15] Choi HL, Albright LD, Timmons MB. An application of the $k-\varepsilon$ turbulence model to predict how a rectangular obstacle in a slot-ventilated enclosure affects air flow. Trans Agric 1990; 33:274–81.

[16] Chen Q. Comparison of different $k-\varepsilon$ models for indoor air flow computations. Numer Heat Transfer Part B 1995; 353–69.

[17] Awbi HB. Application of computational fluid dynamics in room ventilation. Building Environ 1989;24(1):73–84.

[18] Davidson L. Ventilation by displacement in a three-dimensional room: a numerical study. Building Environ 1989;24: 263–72.

[19] Nielsen PV, Restivo A, Whitelaw JH. The velocity characteristics of ventilated rooms. J Fluids Engng 1978;291–8.

[20] Hoff SJ, Janni KA, Jacobson LD. Three-dimensional buoyant turbulent flows in a scaled model, slot-ventilated, livestock confinement facility. Am Soc Agric Engng 1992;35(2): 671–86.

[21] Moureh J, Flick D. Wall air-jet characteristics and airflow patterns within a slot ventilated enclosure. IJTS 2003;42: 703–11.

[22] Wilcox DC. Turbulence modeling for C.F.D. La cañada, CA: DCW Industries, Inc; 1994.

[23] Menter FR. Eddy viscosity transport equations and their relation to the $k-\varepsilon$ model. ASME J Fluids Engng 1997;119: 876–84.

[24] Nallasamy M. Turbulence models and their applications to the prediction of internal flows: a review. Comput Fluids 1987; 151–94.

[25] Launder BE, Reece GJ, Rodi W. Progress in the development of a Reynolds stress turbulence closure. J. Fluid Mech 1975; 68:537–56.

[26] Launder BE, Spalding DB. The numerical computation of turbulent flows. Comput Methods Appl Mech Energy 1974;3: 269–89.

[27] Leonard BP. A stable and accurate convective modeling procedure based on quadratic upstream interpolation. Compt Methods Appl Mech Engng 1979;19:59–98.

[28] Adre N, Albright LD. Criterion for establishing similar air flow patterns (isothermal) in slotted-inlet ventilated enclosures. Trans ASAE 1994;37:235–50.

[29] Yu H, Hoff SJ. Airflow pattern criteria for ceiling slot-ventilated agricultural enclosures under isothermal conditions. Am Soc Agric Engng 1999;42(2):459–69.

[30] Zertal-Ménia N. Etude numérique et expérimentale de l'aéraulique dans un véhicule frigorifique, Thèse INA-PG; 2001.

[31] Nordtvedt T. Cold air distribution in refrigerated trailers used for frozen fish transport. I.I.F./I.I.R. Commissions B1, B2, D1, D2/3, Palmerston North (Nouvelle Zélande) 1993;2:539–44.